Title

Probing the Stability and Band Gaps of Cs2AgInCl6 and Cs2AgSbCl6 Lead-Free Double Perovskite Nanocrystals

Journal

Chemistry of Materials, 31(9)

ISSN

0897-4756

Authors

Dahl, Jakob C
Osowiecki, Wojciech T
Cai, Yao
et al.

Publication Date

2019-05-14

DOI

10.1021/acs.chemmater.8b04202

Peer reviewed

Probing the stability and bandgaps of $Cs_2AgInCl_6$ and $Cs_2AgSbCl_6$ lead-free double perovskite nanocrystals

Jakob C. Dahl,[1,3,4] Wojciech T. Osowiecki,[1,3,] Yao Cai,[2] Joseph K. Swabeck,[1,3] Yehonadav Bekenstein,[1,5] Mark Asta,[2,3] Emory M. Chan,[4] A. Paul Alivisatos[1,2,3,6]

1: Department of Chemistry and 2: Department of Materials Science and Engineering, University of California, Berkeley, California 94720, United States

3: Materials Sciences Division and 4: The Molecular Foundry, Ernest Orlando Lawrence Berkeley National Laboratory, Berkeley, California 94720, United States

5: Department of Materials Science and Engineering, Technion – Israel Institute of Technology, 32000 Haifa, Israel.

6: Kavli Energy NanoScience Institute, Berkeley, California 94720, United States

Abstract:

Lead toxicity has sparked interest into alternative halide nanomaterials with properties similar to $CsPbX_3$ perovskites. A promising alternative suggested from bulk studies is the family of double perovskites of the form Cs_2AgMX_6. Here, we report synthesis of colloidal $Cs_2AgInCl_6$ and $Cs_2AgSbCl_6$ nanocrystals via injection of acyl halides into a metal acetate solution under atmospheric conditions and relatively mild temperatures. We demonstrate the synthesis of single crystalline cubic nanocrystals of ca. 10 nm side length and their morphological similarities to other double perovskite nanostructures in terms of their [200] facet termination and decoration with $Ag^{(0)}$ smaller nanocrystallites. To compare the stabilities of the synthesized materials, we develop a titration assay based on the degradation of nanocrystals with amines as a proxy for degradation by humidity, which provides a quantifiable stability metric. This measurement shows that $Cs_2AgSbCl_6$ releases more than twice the decomposition energy compared to

$Cs_2AgInCl_6$ or $CsPbCl_3$ and degrades in the presence of approximately one molar equivalent of amine, whereas the other two materials require more than a hundredfold excess. Using facile chemical titration to quantitatively determine chemical stability provides an additional tool to aid in the basic understanding of what makes some of these materials more environmentally stable than others.

Introduction:

Metal halide nanocrystals[1,2] are a class of material for which it is possible to create and explore a wide variety of compositions. The prototypical lead system is well-studied because of the attractive optoelectronic properties, which include high photoluminescence quantum yield[3,4] and high tolerance to defects.[5,6] Recent synthetic advances have demonstrated the ability to precisely control the size,[3] shape,[7,8] cation[9,10] and anion[11,12,13] compositions of the nanocrystals to fine-tune the respective band gaps and optical properties.[9,10] Of particular interest from the point of view of solid-state chemistry and nanochemistry are isoelectronic nanocrystal systems[14,15] in which the doubly charged Pb^{2+} ions are replaced by alternating singly and triply charged cations, a crystal structure referred to as double perovskite or elpasolite. Exploration of these systems - and their relative stabilities - offers rich opportunities for learning more about the chemical and physical principles that influence material properties and stability in metal halides.

The investigation of these questions is all the more timely, since the practical application of lead halide perovskite nanocrystals is severely limited by their long-term instability[16] and regulations restricting the use of lead in devices.[17] Identifying environmentally stable, synthetically accessible metal halide nanocrystals that avoid the use of lead while retaining the physical properties of

lead halide perovskite archetypes might allow realization of the many proof-of-concept solar and device applications in development.[18]

Several groups of related materials that substitute lead with other metals have been explored in the recent literature.[19–21] In principle, 3rd- or 4th-row p-block metal halides should have similar electronic structures, due to a potential defect tolerant band structure arising from the Fermi level lying between two antibonding orbitals (mostly composed of metal ns^2 and np^0) and strong spin-orbit coupling.[22] Tin halide and germanium halide perovskites are the closest structural and electronic analogues to lead halide perovskites and are predicted to demonstrate efficient absorption and emission as well as defect tolerance;[22] Unfortunately, these materials are even less stable to light, heat and moisture than lead halide perovskites.[23–26] $Cs_3M_2X_9$ (M = Sb, Bi) and Cs_2MX_6[27] (M = Sn, Pb, Te) structures are ternary metal halide structures that can accommodate p-block metals, and several interesting examples, including Cs_2SnI_6,[28–30] $Cs_3Bi_2I_9$,[31,32] and $Cs_3Sb_2I_9$,[32,33] have been synthesized successfully both in bulk and at the nanoscale. The lower level of structural connectivity of the metal halide octahedra in these structure types reduces conductivity and exciton radii, which may limit their utility in electrical devices. Cs_2AgMX_6 (M = Bi, Sb, In) is a promising structure for lead-free halide perovskites since the metal halide octahedra are connected across all three dimensions.[19] This 3D connectivity may explain why photovoltaic devices made from these materials have exhibited some of the highest power conversion efficiencies reported for lead free halide materials despite the indirect nature of their band gaps.[32,33]

Recently, several groups have reported syntheses of Cs_2AgBiX_6 (X = Br, Cl) nanocrystals.[14,15,34,35] There are discrepancies in reports of optical spectra

between nanocrystal and bulk measurements such as the peak at 430 nm for $Cs_2AgBiBr_6$ which could lead to the interpretation that there is significant quantum confinement in these systems. However, we proposed that these discrepancies arise from differences in measurement technique (transmission vs. reflection) and concentration of the sample instead of from the underlying optical response.[15] This hypothesis received further support from thin film transmission measurements of single-crystalline $Cs_2AgBiBr_6$,[36] which show very similar optical signals to the nanocrystal solutions. In this work, we further elaborate on how these discrepancies may arise and how to eliminate them to ensure comparability between optical absorption measurements from the nanocrystal and solid-state chemistry fields.

Besides Cs_2AgBiX_6, two other silver containing double perovskite crystal structures have recently been reported in bulk: $Cs_2AgSbCl_6$ and $Cs_2AgInCl_6$.[37–39] While neither of these materials are well suited for photovoltaic applications due to their large band gaps, they may have applications in optoelectronic technologies such as the low-noise UV photodetectors recently demonstrated for $Cs_2AgInCl_6$.[40] Here, we report the successful synthesis of $Cs_2AgSbCl_6$ and $Cs_2AgInCl_6$ nanocrystals and investigate their structure, absorption and emission properties. In contrast to a recent report on $Cs_2AgInCl_6$ nanocrystals,[41] we demonstrate that the optical properties of these nanomaterials are mostly unchanged from bulk.

Concerning the understanding of stability, most work has been predicated on the idea that the Goldschmidt tolerance factor[42] can be used as a first guide to predict not only whether a material will form, but also what the stability will be. In recent publications, both thermodynamic measurements[43] and more extensive theoretical calculations or literature comparisons[44,45] support the idea that the

intrinsic stability of these halide systems does indeed correlate well with the Goldschmidt tolerance factor.[41] However, this does not take into account the relative propensity to decompose according to specific pathways. When a perovskite decomposition product consists of metal-ligand complexes, or other molecular species with varied bonding arrangements, the stability of those products can also vary widely across a series of metals, and it is the *net* reaction thermodynamics that are most relevant. The instability of many members of this class of compounds in the presence of water is of particular practical concern. Even slight exposure to humidity is sufficient to decompose materials such as $CsPbI_3$.[46] Many reports include discussions of stability by documenting X-ray diffraction data after a period of storage[38] or immersion of the material in water, ethanol or another solvent.[47,48] In this work, we develop an assay based on an amine degradation reaction observed previously in $CsPbBr_3$ nanocrystals[49] to quantitatively evaluate the stability of $Cs_2AgInCl_6$ and $Cs_2AgSbCl_6$ nanocrystals relative to $Cs_2AgBiCl_6$ and $CsPbCl_3$. We demonstrate that $Cs_2AgSbCl_6$ decomposes with a 1000-fold lower amine concentration than $Cs_2AgInCl_6$ and extract both equilibrium constants and free reaction energies from an equilibrium model of the data.

Experimental Methods:

Materials:

Acetone (99.9%, Fischer Scientific), Antimony (III) acetate (99.99%, Aldrich), Benzoyl chloride (99%, VWR), Bismuth (III) acetate (99.99%, Aldrich), Cesium Acetate (99.9% Aldrich), Cesium standard for ICP (1000 ppm in 2% aqueous nitric acid, Aldrich, TraceCert Lot: BCBK9448V), 2% aqueous nitric acid (Aldrich, 99.999%) , 2-ethylhexanoyl chloride (98%, Aldrich), Hexanes (mixture of isomers 99.99 %, Fischer Scientific), Indium (III) acetate (99.99%, Aldrich), Lead (II)

acetate Trihydrate (99.99%, Aldrich), Octylamine (99%, Aldrich), Oleic Acid (90%, Aldrich), Oleylamine (70%, Aldrich), Silver Acetate (99.99%, Aldrich) and m-Xylene (99.9%, Fischer Scientific). All chemicals were used as purchased without further purification.

Synthesis of $Cs_2AgInCl_6$ nanocrystals:

In a typical synthesis, 5 mg (0.025 mmol) cesium acetate, 8 mg (0.05 mmol) silver acetate and 16 mg (0.05 mmol) indium (III) acetate were placed into a 4 mL glass vial with a stir bar. Xylene (1 mL), oleic acid (0.25 mL, 0.8 mmol) and oleylamine (0.075 mL, 0.2 mmol) were added, and the vial heated to 100 °C for 10 minutes in an oil bath. Benzoyl chloride (0.040 mL, 0.3 mmol) was injected quickly. Then, the vials were taken out of the oil bath and left to cool to room temperature. The cooling rate and precise time of removal after injection did not appear to have any major effects on result of this synthesis. For routine measurements, the nanocrystal reaction mixture was precipitated by centrifugation at 14,000 rpm for 5 minutes and the resulting pellet was re-dispersed in hexanes.

Synthesis of $Cs_2AgSbCl_6$ nanocrystals:

A typical synthesis of $Cs_2AgSbCl_6$ nanocrystals started with 5 mg (0.025 mmol) cesium acetate, 3 mg (0.02 mmol) silver acetate and 17 mg (0.05 mmol) antimony (III) acetate in a 4- mL glass vial with stir bar. Liquid reagents including Xylene, oleic acid (0.4 mL, 1.3 mmol) and oleylamine (0.075 mL, 0.2 mmol) were added next, then the vial was plunged into an oil bath at 100 °C for one minute. An acyl chloride, 2-ethyl 2-hexanoyl chloride (0.100 mL, 0.6 mmol) was injected quickly, and the vials were taken out of the oil bath and left to cool to room temperature and worked up in the same way as the $Cs_2AgInCl_6$ nanocrystal

mixture. $Cs_2AgSbCl_6$ metal halide and surfactant precursor mixtures that were heated for more than a minute, or left stirring under argon at room temperature for a prolonged period of time developed a reddish-brown tint and did not yield nanocrystals.

Procedures for $CsPbCl_3$ and $Cs_2AgBiCl_6$ nanocrystals are similar to the procedure for $Cs_2AgInCl_6$ nanocrystals and can be found in the SI.

Absorption Measurements

For dilute absorption measurements, approximately 10 - 100 µL of nanocrystal solution was added to a quartz cuvette containing 3 mL of hexanes and measured in a Shimadzu UV-3600 UV−vis−NIR spectrophotometer. To measure the band edge, the entire concentrated nanocrystal solution was placed in a quartz cuvette and measured in the same spectrophotometer. Then, the absorbance was converted to absorptance, and either the square root (for indirect bandgaps in $Cs_2AgSbCl_6$) or the square (for direct bandgaps in $Cs_2AgInCl_6$) of this value was plotted against energy[50]. A straight line was fit to the linear part of this function, and the x-axis intercept was reported as the band gap. The errors of the band gap were propagated from the fitting errors in the parameters of the line equation.

Photoluminescence and Photoluminescence Excitation Measurements

A concentrated nanocrystal solution was placed in a quartz cuvette, and spectral photoluminescence and photoluminescence excitation measurements were taken on an Edinburgh FLS 980 Spectrometer. The photoluminescence quantum yield of $Cs_2AgInCl_6$ was measured at an excitation of 300 nm wavelength in an Edinburgh spectrometer equipped with an integrating sphere. The light out of the

integrating sphere was integrated between 480-840 nm for emission and between 275 and 325 nm for absorption.

Transmission Electron Microscopy (TEM) One drop of dilute nanocrystal solution (prepared for optical measurements, 1:30 dilution) was cast onto a TEM grid (EMS, CF400-Cu). The samples were observed with 200 kV Tecnai G2 T20 S-TWIN with a Gatan SC200 CCD camera.

X-ray Diffraction

The nanocrystal solution in hexanes was further concentrated by evaporating with a flow of nitrogen. This concentrate was drop-cast onto a low-background substrate and the X-ray beam focused on the resulting film. Measurements were taken using a GADDS D-8 Series 1 Diffractometer equipped with a Vantec 500 detector, and on a D2 Phaser equipped with a Silicon SSD 160 detector.

Scanning Transmission Electron Microscopy and Energy Dispersive X-ray Spectroscopy (STEM-EDS)

Samples were investigated with FEI TitanX operating at 120kV, using a Fischione high-angle annular dark-field (HAADF) detector with an inner semiangle, β, of 63 mrad. The STEM-EDS measurement was then initiated and averaged over 3-4 minutes for every image, and the characteristic X-ray Fluorescence of each material analyzed using modified Cliff-Lorimer Factors in the Bruker Esprit program. (Details in SI)

Cs GF-AAS concentration measurements

About 1 mL of each nanocrystal stock solution was dried in a vial. High-purity aqueous nitric acid (2%) was added, and the vial sonicated for 20 minutes. The resulting solutions were weighed and diluted 20,000 times in 2% nitric acid. A 1000 ppm Cs standard solution was diluted 20,000, 50,000, and 200,000 times. These dilutions were used to create a calibration curve, against which the other samples were measured. The solutions had a Cs concentration of 6.194, 6.316, 18.03 and 13.37 ppb for $Cs_2AgSbCl_6$, $Cs_2AgBiCl_6$, $Cs_2AgInCl_6$ and $CsPbCl_3$, respectively, and these concentrations were used to calculate the molar absorptivity of the original nanocrystal solutions to keep the concentration approximately the same between the different nanocrystals for comparison in the amine degradation assay (Figure S6).

Amine degradation assay:

Diluted solutions of amines (0.00001 – 0.1 M in dodecane) were added to nanocrystal solutions (0.3 mM in dodecane). The absorption was monitored with a Biotek Synergy 4 plate reader until it stopped changing (approx. 4 hours). A background absorption spectrum of pure dodecane was subtracted from all samples, then each measurement was fitted to a scattering fraction based on the absorption from 450-600 nm and a nanocrystal absorption fraction. The resulting nanocrystal absorptions were divided by the initial absorption in each sample to calculate the fraction of material remaining, and the data was fitted to an equilibrium equation (Details in SI).

Theoretical Calculations:

All structure relaxations were carried out employing spin-polarized PBE-GGA[51] based DFT methods, as implemented in the Vienna ab-initio simulation package (VASP)[52]. For the calculations involving molecules, we employ periodic supercells

which are carefully tested for energies to be converged (with respect to system size, i.e., to remove artifacts of interactions with periodic images) to within 0.2 meV/atom. The exciton radius (R) was computed within the Wannier-Mott model[53], using the expression $R = \frac{\varepsilon a_0}{m^*}$, where m^* is the reduced exciton mass ($\frac{1}{m^*} = \frac{1}{m_e} + \frac{1}{m_h}$), a_0 is the Bohr radius, and ε is the dielectric constant of the material. For the dielectric constant, we considered only the contribution from electronic polarization, i.e., taking the high-frequency contribution, assuming $\varepsilon = \varepsilon_\infty$. The dielectric constant was calculated by means of density functional perturbation theory, as implemented in Vienna Ab initio Simulation Package (VASP)[54]. The average effective mass was calculated using VASP and the methodology implemented in the BoltzTrap code[55] (details in SI).

Results and Discussion:

To synthesize $Cs_2AgSbCl_6$ and $Cs_2AgInCl_6$ nanocrystals, we adapt a recent method employing an injection of acyl halides into a solution of metal acetate precursors[56] rather than adding cesium oleate to a solution of metal halides.[3] Briefly, in an open vial under atmospheric conditions, metal acetates are added to a solution of xylene, oleic acid and oleylamine, heated to 100 °C, then an acyl halide is injected (Figure 1). This substitutes the water- and air-sensitive antimony (III) chloride with the more stable antimony (III) acetate as a precursor and provides more tunability over the reaction by enabling the change of type or concentration of acyl halide. The reaction reaches completion after less than one minute, and nanocrystals are separated from the reaction solution through centrifugation and redispersion. To showcase the broad utility of this synthesis,

we also make $Cs_2AgBiCl_6$ and $CsPbCl_3$ using the same method, which show similar properties as previously reported nanocrystals (Figure S9).

For the synthesis of $Cs_2AgSbCl_6$, the control afforded by acyl halide injection is crucial: the addition of an equimolar amount of benzoyl chloride leads to formation of lamellar structures or stacks of small plates, while two equivalents produce a mixture of nanoplatelets and nanocubes; when a more reactive precursor, 2-ethylhexanoyl chloride, is added instead, nanocubes form (Figure S10). This behavior bears some resemblance to the influence of the temperature on the synthesis of $CsPbBr_3$ nanocrystals, with similar lamellar structures found at very low temperatures, which then transition to plates and cubes as the temperature rises.[7] It is possible that the decomposition kinetics of the acyl halide precursor could control the shape of the crystal through a growth instability arising from the competition of nucleation islands on facets of different size, similar to recent reports on the formation of CdSe nanoplatelets.[57] Slower kinetics may allow the formation of plates or even lamellar structures when the difference in activation barrier to form a new layer on a smaller crystal facet instead of a larger crystal facet is a significant part of the overall energetic process; faster kinetics may overwhelm this difference in activation energy, causing isotropic shapes at higher temperatures, higher concentrations of the halide species or with a more reactive halide precursor.

Structurally, both $Cs_2AgInCl_6$ and $Cs_2AgSbCl_6$ nanocrystals appear to exhibit only the elpasolite or double perovskite $F_{m\text{-}3m}$ structure in powder X-ray diffraction measurements of nanocrystal thin films, as determined by comparing the peak positions to the bulk $F_{m\text{-}3m}$ phase of $Cs_2AgInCl_6$ and $Cs_2AgSbCl_6$ (Figure 2). Orientation effects appear to change the relative peak intensities in the

nanocrystal thin films we measure compared to the bulk phase. Under some synthesis conditions, we observe AgCl impurities, which can be removed following synthesis through careful centrifugation and redissolution of the nanocrystals in the case of $Cs_2AgInCl_6$, but not for $Cs_2AgSbCl_6$. We eliminated impurities in $Cs_2AgSbCl_6$ by changing the ratio of M (III) to Ag (I) precursor (Figure S2). Due to the negligible optical response in the region important for $Cs_2AgSbCl_6$, we can measure the properties of $Cs_2AgSbCl_6$ nanocrystals without interference in a mixed sample of AgCl and $Cs_2AgSbCl_6$ nanocrystals (see SI for a more thorough discussion of the AgCl impurity).

In transmission electron microscopy (TEM) images, we observe cubic nanocrystals with edges approximately 10 nm in length and a size dispersion of about 15%. There is close agreement between sizes determined by TEM (Figure S11) and from Scherrer analysis of X-ray diffraction (XRD) patterns (Figure S12, Table S1)) for $Cs_2AgInCl_6$ crystals (Figure 2) and for $Cs_2AgSbCl_6$ crystals with AgCl impurity (Figure S2) synthesized under similar conditions as the $Cs_2AgInCl_6$ crystals. $Cs_2AgSbCl_6$ nanocrystals synthesized in a phase pure manner were larger and less monodisperse (Figure 2).

High-resolution TEM images of $Cs_2AgInCl_6$ nanocrystals display a lattice spacing of 0.37 nm corresponding to a [220] plane. For $Cs_2AgSbCl_6$ nanocrystals, we observe 0.38 and 0.45 nm lattice spacings that correspond well to [220] and [200] planes, respectively. The correspondence of the lattice spacings throughout the crystal to high-reflectivity, low-index planes supports the claim that these nanocrystals are phase pure and single crystalline. The orientation of these planes relative to the edges further suggests that the cubes are terminated by [200] facets, similar to reports on lead halide perovskites[3] as well as our recent results on Cs_2AgBiX_6 double perovskites.[15] The elemental ratios from scanning transmission electron microscopy energy dispersed X-ray

spectroscopy (STEM-EDS) measurements is consistent with expected values (Figure S13), and the ions appear co-localized in the material. We also observe small $Ag^{(0)}$ nanocrystallites decorating the cubes, which suggests similarities in the degradation process of silver-containing double perovskites. In our previous work with $Cs_2AgBiBr_6$, we demonstrated that these smaller silver nanocrystallites grow during the growth reaction itself, and not subsequently during analysis through an interaction with the TEM beam.[15] Likewise, in these materials, we do not observe a significant growth of the nanocrystallites during ~5 min STEM-EDS mapping experiments (300pA/nm exposure), though some migration and coalescence do occur (Figure S14). From structural characterization we conclude that the synthesized particles are single crystalline, cubic double perovskite nanocrystals around 10 nm in size, terminated by [200] facets and decorated with $Ag^{(0)}$ nanocrystallites.

Having ascertained the nature of the double perovskite nanocrystals, we investigate their optical properties, which serve as a probe of the degree of quantum confinement. We observe that the absorption spectra of the nanocrystal solutions have a rising shoulder from 310-290 nm for $Cs_2AgInCl_6$ nanocrystals (Figure 3) as reported previously[41] and peaks at 360 and 300 nm for $Cs_2AgSbCl_6$ nanocrystals, which are both significantly removed from the reported bulk band edge.[39] The dual absorption peaks for $Cs_2AgSbCl_6$ nanocrystals are similar to the shape of reflectometry peaks found in bulk samples.[39] A Tauc analysis[50] on absorption spectra of dilute solutions of $Cs_2AgSbCl_6$ and $Cs_2AgInCl_6$ nanocrystals indicates band gaps of 2.83 ± 0.02 and 4.15 ± 0.05 eV, respectively (Figure S 16). This is a significant blue-shift from the reported bulk band gaps of 2.5 and 3.5 eV,[39] which at first glance would lead to the conclusion that both nanocrystals show significant quantum confinement. However, we do

not observe a corresponding blue shift of the broad emission of $Cs_2AgInCl_6$ (< 0.1 eV) compared to the emission in bulk.[37] The photoluminescence quantum yield of $Cs_2AgInCl_6$ nanocrystals was measured to be 0.6 %, which is within measurement error of the quantum yield reported previously.[41] In addition, confined structures of $Cs_2AgSbCl_6$, such as the small nanoplates in Figure S10, do not show a blue-shift of either the shoulder at 360 nm or the peak at 300 nm, as would be characteristic for a quantum confined exciton peak. The excitation spectrum of this emission decays into background at approximately 350 nm or 3.5 eV. This band edge is 0.7 eV lower than the calculated band gap from absorption measurements, but nearly identical to the bulk bandgap. These different optical measurements do not agree with each other, with absorption spectra suggesting a confinement energy of 0.7 eV for $Cs_2AgInCl_6$ and 0.3 eV for $Cs_2AgSbCl_6$, while emission and excitation spectra of $Cs_2AgInCl_6$ suggest less than 0.1 eV of confinement. Turning to density functional theory to investigate which level of confinement one should expect in the different double perovskites, we calculate the effective electron and hole masses and dielectric constants (Table S2). The resulting exciton Bohr radii, 1.02 nm for $Cs_2AgSbCl_6$ and 0.82 nm for $Cs_2AgInCl_6$ are an order of magnitude smaller than the size of the crystals, strongly suggesting that quantum confinement should be minimal in both materials.

Since the absorption spectra are the only measurements supporting the interpretation of strong quantum confinement, we considered the differences in measurement conditions between bulk and nanocrystal to enable a more confident measurement and analysis of bandgaps in nanocrystals in the cases where there is no emission and excitation data, such as in $Cs_2AgSbCl_6$. Bandgaps of bulk materials are commonly calculated from Tauc plots made with data obtained by reflection measurements of pure powders, while colloidal nanocrystals are measured in dilute solutions in transmission mode and have

historically not been analyzed with Tauc plots. The difference in concentration is large, changing from pure material in bulk to an optically dilute sample for nanocrystals, a range of three orders of magnitude in the number of unit cells sampled. Preparation of nanocrystal solution samples is usually quite dilute to enable peak analysis of the most strongly absorbing species. As the variation in peak extinction coefficients of transition metal complexes (up to seven orders of magnitude)[58] exceeds the dynamic range of most absorption spectrometers (0.001– 4 absorbance units in the instrument we utilize), it stands to reason that spectra optimized for observing the strongest absorption peaks in nanocrystals may have insufficient signal to accurately measure the absorption at the band edges for weakly absorbing bands. In this particular case, the band-edge absorption features are indeed expected to be weak since the transitions close to the band edge should be Laporte forbidden for $Cs_2AgInCl_6$ due to the 4d - 5 s transition at the band edge[40] and momentum forbidden for $Cs_2AgSbCl_6$ due to the indirect bandgap.[39]

To overcome these problems and more accurately measure the absorption at the band edges of $Cs_2AgInCl_6$ and $Cs_2AgSbCl_6$ nanocrystals, we perform Tauc analysis using absorption spectra of nanocrystal solutions that are 300 times more concentrated than those used to observe the absorption maxima. Although these spectra do not provide information on transitions that lie higher in energy due to the noise limit of the detector, this scheme is necessary to obtain precise linear fits of the absorptance spectra at the weakly absorbing band edges. The Tauc analysis of concentrated nanocrystal absorption spectra results in band gaps consistent with those measured for bulk samples,[38,39] with an indirect gap of 2.57 ± 0.05 eV for $Cs_2AgSbCl_6$ and a direct gap of 3.57 ± 0.03 eV for $Cs_2AgInCl_6$.

One possible concern when using concentrated colloidal solutions for Tauc analysis is that lower-bandgap impurities may confound the measurement.

However, since the Tauc plot is designed to ignore low probability contributions at lower energies, such as the Urbach tail, it is also insensitive to contamination by lower-bandgap impurities, since the slope of any impurity absorptions that are not at their band edge in Tauc plots is significantly different than the slope for the band edge. A good test case is the analysis of $Cs_2AgSbCl_6$ (Figure 3C): There is a small-bandgap impurity of unknown origin in the $Cs_2AgSbCl_6$ spectrum, visible in the deviation of the spectrum from the baseline below the bandgap of $Cs_2AgSbCl_6$. Despite the evident impurity, it is possible to assign the slopes to different materials, allowing for an unambiguous identification of the band gap. We therefore confirm that Tauc analysis can be a valuable tool in analyzing energies of band gaps in nanocrystals, if appropriate measurement conditions are chosen. From our optical and theoretical analysis, we further conclude that both $Cs_2AgInCl_6$ and $Cs_2AgSbCl_6$ have close to no quantum confinement at the length scale synthesized and are unlikely to exhibit much confinement unless the size is drastically decreased.

The instability of metal halide nanocrystals in the presence of polar molecules has been widely acknowledged as a significant obstacle to many applications.[47] Despite this recognition, there are few methods to measure and compare the relative stability of metal halide nanocrystals. We sought a robust and quantitative measure of perovskite nanocrystal stability, so we developed a decomposition titration assay in which $Cs_2AgSbCl_6$, $Cs_2AgInCl_6$, $Cs_2AgBiCl_6$ and $CsPbCl_3$ nanocrystals are titrated with amines. This assay is based on decomposition reactions of halide perovskites with amines previously observed in the case of $CsPbBr_3$[49,59–61] and $Cs_2AgBiBr_6$[15] nanocrystals. Reactions with amines serve as a more reproducible proxy for the stability of perovskite nanocrystals than direct exposure to water, since amines and water are similar in hardness,

but amines are miscible with nonpolar colloidal solutions of halide nanocrystals. In the decomposition reaction of $CsPbBr_3$ to Cs_4PbBr_6, it has been proposed that three units of $PbBr_2$ from every four unit cells react with amines to form a complex in solution, leaving behind lead-depleted nanocrystals[49]. For the double perovskites, STEM-EDS analysis of the depleted products after amine degradation reveals trace amounts of Sb, Bi or In, leaving large aggregates containing Cs, Ag and Cl (Figures S11-S13). The concentration of double perovskite unit cells converges to a fixed non-zero value after being exposed to an excess of amine-containing solutions during the time scale of the reaction. This suggests the possibility that the metal-ligand complexes and other molecular species reach a quasi-equilibrium with the nanocrystals in solution. The degradation process is a complex process on the individual nanocrystal level, and nanocrystals of both double perovskite and perovskite compositions appear to etch, grow and fuse at the same time (Figure S23). Nevertheless, on the macroscopic level this process appears reversible, as demonstrated previously for $CsPbBr_3$ nanocrystals through heat or addition of oleic acid.[61] Since we cannot remove amines or nanocrystals from the solution without substantially altering the reaction, we reduce the number of amines available chemically. By protonating the amine by adding oleic acid in excess of that already present as surfactant in the nanocrystal solution, we couple the equilibrium of nanocrystals with amine to an acid-base equilibrium of the amine with oleic acid. This allows us to reverse some of the degradation of double perovskite nanocrystals and suggests reversibility of the nanocrystal degradation reaction at room temperature (Figure S28).

We therefore propose the following reaction with amines for all double perovskites (M = Sb, In, Bi):

$$Cs_2AgMCl_6 + RNH_2 \rightleftharpoons MCl_3RNH_2 + Cs_2AgCl_3 \quad (1)$$

To measure the degradation behavior of the above reaction, amines are titrated into solutions of nanocrystals in dodecane and the change in absorption from the original solution is measured. For the materials examined here, $Cs_2AgSbCl_6$ dissolves in the presence of the lowest concentrations of octylamine (0.01 – 0.1 mM), while $Cs_2AgBiCl_6$ dissolves at a higher concentration (~1 mM) and $Cs_2AgInCl_6$ and $CsPbCl_3$ require still higher concentrations (~10-100 mM) (Figure 4). These materials can be characterized and compared by the concentration of amine required to degrade a defined fraction of the sample. This point is defined as the 1/e point in our analysis (see Table 1). Based on some of our observations as well as prior publications on $CsPbBr_3$,[61] we postulate that this reaction is in quasi-equilibrium. Under this assumption, we developed a simplified equilibrium model, which we use to fit the data to a model equilibrium constant. The decomposition of several different materials can be well fit with this simplified equilibrium equation, lending additional support to the idea that an equilibrium reaction is occurring. Based on the proposed reaction equation (Equation 1), we rewrite the equilibrium equation by replacing the concentration of product by the difference between initial and current concentrations of starting material so that the equilibrium constant is expressed entirely by the fraction of starting material remaining and the initial concentration of amines and nanocrystal unit cells:

$$K = \frac{(X_0 - f_i * X_0)}{f_i * X_0 - [L_0 - (X_0 - f_i * X_0)]} \quad (2)$$

Where K is the equilibrium constant, X_0 is the initial concentration of double perovskite, f_i is the fraction of starting material remaining and L_0 is the initial concentration of amines. In our experiment, $f_i = X/X_0$ is determined as the fraction of the initial absorption remaining (abs/abs_i). The equilibrium equation

with one amine binding one metal-halide most consistently fit the absorption data (Figure S27); this suggests the $1/L_0$ dependence used in the equation.

The absorption data in the decomposition curves are fit to this equilibrium equation model and equilibrium constants for each of the nanocrystals are extracted. This equilibrium model is undoubtedly an oversimplification of a complex process involving reactions at different time and length-scales, but it is consistent with the observations, and allows us to quantitatively compare the relative stability of these materials. While the errors on the extracted equilibrium constants are substantial, the differences between the various equilibrium constants are separated by at least one standard error, with exception of the constants of $CsPbCl_3$ and $Cs_2AgInCl_6$, which are close to identical. Using the fitted equilibrium constants, the standard Gibbs free energy of reaction can also be estimated through $\Delta G° = -RTlnK$ (Table 1). The large and negative free energy values agree with the spontaneous occurrence of these reactions in dilute solution at room temperature as well as with the large extracted equilibrium constants.

To verify that the results of the amine titrations are reasonable proxies for real stability differences under atmospheric humidity, we measured the degradation of TEM samples in atmospheric moisture. $Cs_2AgSbCl_6$ placed on a TEM grid degrades into a Sb-depleted phase in a matter of hours, while $Cs_2AgInCl_6$ is stable under atmospheric conditions for more than a week (Figure S29). Additionally, the $Cs_2AgSbCl_6$ nanocrystals degrade under standard beam conditions during STEM-EDS measurement (Figure S30), and STEM-EDS measurements of the $Cs_2AgSbCl_6$ nanocrystals exposed to air for more an hour show a significant depletion of Sb content in the crystals, with a corresponding

accumulation of amorphous Sb-containing agglomerations outside of the crystals (Figure S31). The difficulty of purifying AgCl from $Cs_2AgSbCl_6$ might also arise in part from the instability of the parent material, potentially causing some degradation to AgCl during purification.

Based on the quantitative data on the stability of these three compounds, we now consider three different factors which could potentially explain the difference in stability between cesium silver chloride double perovskites (Table 1 and Table S3): (1) The Goldschmidt tolerance factor, (2) the stability of the crystal as measured by crystal formation energies, or (3) the binding affinity of the p-block metals for the amines over chlorides, which should correlate to the hardness of the metal. The Goldschmidt tolerance factor as well as more complicated radius ratio fits that include both the tolerance factor and octahedral radius ratios do not explain the observed trends in stability. While crystal stability correlated well with the melting point of the binary halides as well as with the standard heats of formation from the elements, the difference in crystal formation energies from the lowest energy starting materials, ΔH_f , which is a more direct measure of the intrinsic crystal stability,[43] did not correlate with the measured stability at all. The Pearson hardness[62] of the elements correlates well with the degradation energy, with Sb, the hardest acid, releasing the most energy during a reaction with the hard amine base and In as the softest acid releasing the least. However, other possible measures, such as the hardness of the ions, of the metal halide complexes or solubility might better described this interaction. To better understand and predict the stability in complex metal halide materials to the wide variety of environmental perturbations, such as humidity, heat, light, electrical current and others, more experimental and theoretical studies comparing materials in a quantifiable manner are needed. We

anticipate that the method presented here could aid in the quantification of the stability of metal halide materials.

Conclusion:

In this report, we demonstrate a colloidal synthesis of nanocrystals of $Cs_2AgInCl_6$ and $Cs_2AgSbCl_6$ using a robust, tunable method of injecting acyl halides under atmospheric conditions and relatively mild temperatures. We identify the type and concentration of acyl halide as an easily tunable variable that profoundly affects the synthetic outcome. The particles synthesized are crystalline nanocubes of 10 nm edge length terminated with [200] facets and decorated with silver particles. We show that the optical properties remain unchanged from bulk despite the appearance of dilute absorbance spectra and discuss the need to prepare concentrated optical samples for accurate Tauc analysis of nanocrystals. We develop a degradation assay for the nanocrystals and show a decrease in chemical stability from $Cs_2AgInCl_6$ over $Cs_2AgBiCl_6$ to $Cs_2AgSbCl_6$. This ability to quantitatively measure perovskite environmental stability can enhance the understanding of metal halide materials, accelerate the identification of more stable perovskite analogues, and enable the elucidation of design rules for the environmental stability of a broad range of metal halide semiconductor nanocrystals.

The authors declare no conflicts of interest.

Acknowledgements

All experimental work was supported by the U.S. Department of Energy, Office of Science, Office of Basic Energy Sciences, Materials Sciences and Engineering Division, under Contract No. DE-AC02-05-CH11231 within the Physical Chemistry

of Inorganic Nanostructures Program (KC3103). The STEM-EDS and amine degradation measurement work at the Molecular Foundry was supported by the Office of Science, Office of Basic Energy Sciences, of the U.S. Department of Energy under Contract No. DE-AC02-05-CH11231. All theory calculations were supported by the U.S. Department of Energy, Office of Science, Office of Basic Energy Sciences, Materials Sciences and Engineering Division under Contract No. DE-AC02-05-CH11231 within the Materials Project program (KC23MP). J.C.D. acknowledges support by the National Science Foundation Graduate Research Fellowship under DGE 1752814. Y.C. was funded by the National Research Foundation (NRF), Singapore (CRP NRF2014NRF-CRP002-036), and the Singapore-Berkeley Research Initiative for Sustainable Energy (SinBeRISE) CREATE program. The authors acknowledge QinQin Yu, Brent Kosher, Arunima Balan, Justin Ondry, Dante Valdez, Dr. Karen Bustillo, Dr. Assaf Ben Moshe, Dr. Ayelet Teitelboim and Dr. Myoungwhan Oh for fruitful discussions.

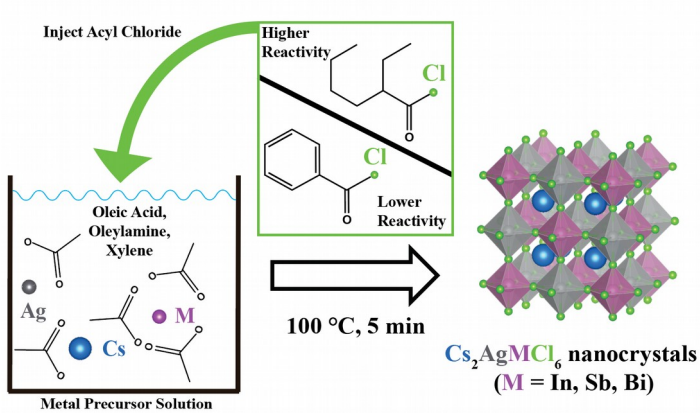

Figure 1: Reaction scheme for the synthesis of double perovskite nanocrystals. A solution of metal acetates (cesium, silver and indium, antimony or bismuth) in xylene with oleic acid and oleylamine is heated to 100 °C, then an acyl chloride precursor is injected to form nanocrystals of the corresponding Cs_2AgMCl_6 (M = In, Sb, Bi) double perovskite. The reactivity of the acyl chloride precursor is an important factor for tuning nanocrystal formation.

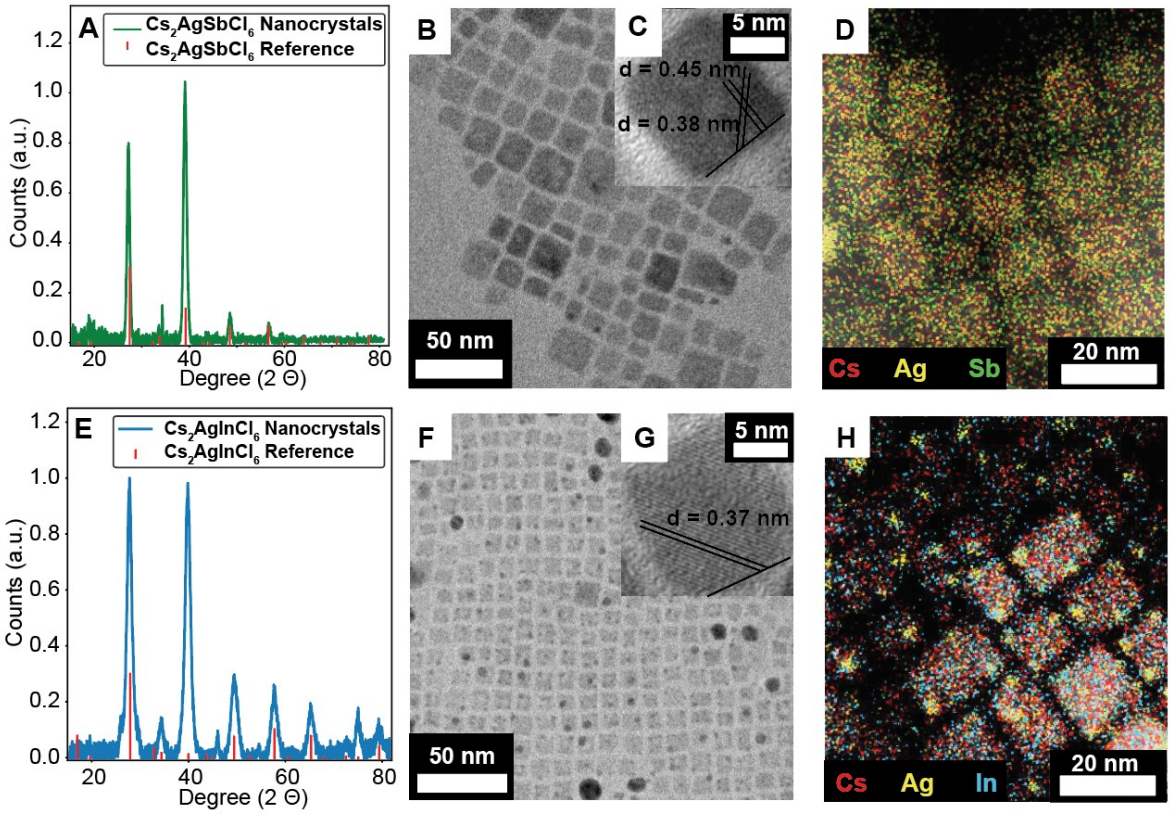

Figure 2: Structural characterization of $Cs_2AgSbCl_6$ (A-D) and $Cs_2AgInCl_6$ nanocrystals (E-H). (A) XRD pattern of nanocrystals measured with a Co source (λ = 1.7789 Å) with references COD 1546185 ($Cs_2AgSbCl_6$) (B) TEM image showing cubic nanocrystals (C) HR-TEM image of a nanocube on a [100] zone axis showing 0.45 nm ([200]) lattice planes parallel to the edge of the cube and 0.38 nm ([220]) planes diagonal to the edge of the cube and (D) STEM-EDS map of $Cs_2AgSbCl_6$ showing co-localization of cations. (E) XRD pattern of nanocrystals measured with a Co source (λ = 1.7789 Å) with reference COD 1546186 ($Cs_2AgInCl_6$) (F) TEM image showing cubic nanocrystals. (G) HR-TEM image of a nanocube on a [100] zone axis showing 0.37 nm ([220]) lattice planes diagonal to the edge of the cube, and (H) STEM-EDS map of $Cs_2AgInCl_6$ showing co-localization of cations as well as silver spots.

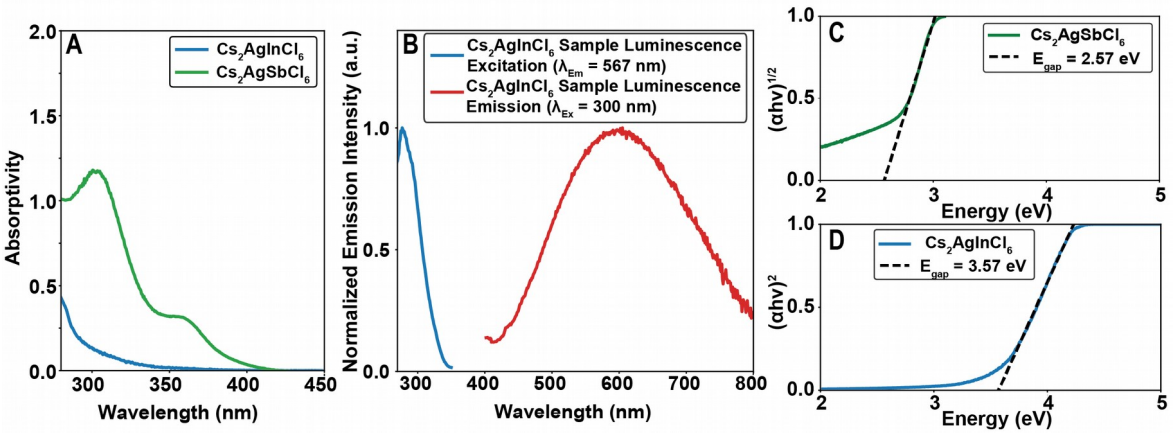

Figure 3: Optical Properties of $Cs_2AgSbCl_6$ and $Cs_2AgInCl_6$ nanocrystals. (A) UV-Visible absorption spectra of $Cs_2AgSbCl_6$ and $Cs_2AgInCl_6$ nanocrystals, with peaks centered at 360 nm and 300 nm for $Cs_2AgSbCl_6$ and no discernible peak for $Cs_2AgInCl_6$. (B) Photoluminescence (PL) and photoluminescence excitation (PLE) spectra of $Cs_2AgInCl_6$ samples. The maximum PL occurs at 550 nm, the maximum PLE at 300 nm. (C) Tauc plot of the absorption spectrum of concentrated $Cs_2AgSbCl_6$ nanocrystals showing an indirect bandgap of 2.57 ± 0.05 eV. (D) Tauc plot of absorption spectrum of concentrated $Cs_2AgInCl_6$ nanocrystals showing a direct bandgap of 3.57 ± 0.03 eV.

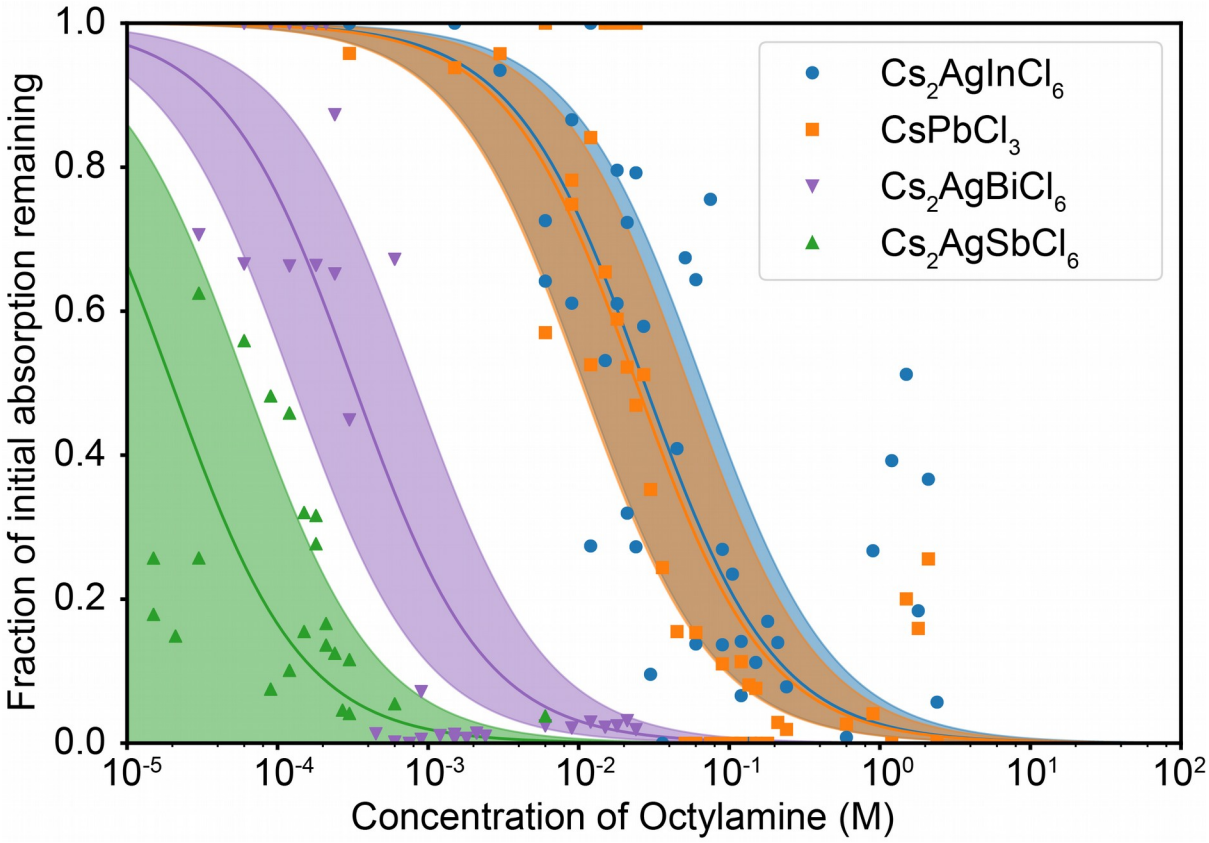

Figure 4: Stability analysis $Cs_2AgSbCl_6$, $Cs_2AgBiCl_6$, $Cs_2AgInCl_6$ and $CsPbCl_3$ nanocrystals. Individual points represent the fraction of initial absorption remaining after 4 hours as a function of the different concentrations of octylamine that the nanocrystal solutions were exposed to. The solid lines are fits of the data points to an equilibrium equation (Equation 2), while the shaded regions represent 1σ confidence intervals for those fits.

Compound	$Cs_2AgSbCl_6$	$Cs_2AgBiCl_6$	$Cs_2AgInCl_6$
K_{eq}	5×10^{5}	3×10^{3}	40
Δ G° (kJ/mol)	-27	-20	-9
1/e point (M)	9×10^{-5}	4×10^{-4}	4.4×10^{-2}

Table 1: Results of decomposition analysis. Equilibrium constants are based on fits to optical absorption data of the degradation reaction (Figure 4). We calculate the equilibrium constant based on the assumption that all activity coefficients are equal to 1. The number reported here is technically not an equilibrium constant but rather a concentration ratio with units of M^{-1}. Standard Gibbs enthalpies of reaction are calculated based on the equilibrium constants. The 1/e point is the characteristic point at which 1/e of the initial concentration of unit cells remains. It is calculated based on the linear fit in the log-log plot (Figure S27) and does not rely on the equilibrium model.

Supporting information:

Synthesis procedures used for $CsPbCl_3$, $Cs_2AgBiCl_6$, AgCl and monodisperse $Cs_2AgSbCl_6$ nanocrystals with AgCl impurities, discussion of AgCl impurities, further elaboration of Tauc analysis and amine degradation analysis, and STEM-EDS analysis.

References:

(1) Kovalenko, M. V; Protesescu, L.; Bodnarchuk, M. I. Properties and Potential Optoelectronic Applications of Lead Halide Perovskite Nanocrystals. *Science (80-.).* **2017**, *358*, 745–750.

(2) Akkerman, Q. A.; Rainò, G.; Kovalenko, M. V.; Manna, L. Genesis, Challenges and Opportunities for Colloidal Lead Halide Perovskite Nanocrystals. *Nat. Mater.* **2018**, *17*, 394–405.

(3) Protesescu, L.; Yakunin, S.; Bodnarchuk, M. I.; Krieg, F.; Caputo, R.; Hendon, C. H.; Yang, R. X.; Walsh, A.; Kovalenko, M. V. Nanocrystals of Cesium Lead Halide Perovskites (CsPbX3, X = Cl, Br, and I): Novel Optoelectronic Materials Showing Bright Emission with Wide Color Gamut. *Nano Lett.* **2015**, *15*, 3692–3696.

(4) Koscher, B. A.; Swabeck, J. K.; Bronstein, N. D.; Alivisatos, A. P. Essentially Trap-Free CsPbBr 3 Colloidal Nanocrystals by Postsynthetic Thiocyanate Surface Treatment. *J. Am. Chem. Soc.* **2017**, *139*, 6566–6569.

(5) Brandt, R. E.; Poindexter, J. R.; Gorai, P.; Kurchin, R. C.; Hoye, R. L. Z.; Nienhaus, L.; Wilson, M. W. B.; Polizzotti, J. A.; Sereika, R.; Žaltauskas, R.; et al. Searching for “Defect-Tolerant” Photovoltaic Materials: Combined Theoretical and Experimental Screening. *Chem. Mater.* **2017**, *29*, 4667–4674.

(6) Kang, J.; Wang, L.-W. High Defect Tolerance in Lead Halide Perovskite CsPbBr $_3$. *J. Phys. Chem. Lett.* **2017**, *8*, 489–493.

(7) Bekenstein, Y.; Koscher, B. A.; Eaton, S. W.; Yang, P.; Alivisatos, A. P. Highly Luminescent Colloidal Nanoplates of Perovskite Cesium Lead Halide and Their Oriented Assemblies. *J. Am. Chem. Soc.* **2015**, *137*, 16008–16011.

(8) Akkerman, Q. A.; Motti, S. G.; Srimath Kandada, A. R.; Mosconi, E.; D’Innocenzo, V.; Bertoni, G.; Marras, S.; Kamino, B. A.; Miranda, L.; De Angelis, F.; et al. Solution Synthesis Approach to Colloidal Cesium Lead Halide Perovskite Nanoplatelets with Monolayer-Level Thickness Control. *J. Am. Chem. Soc.* **2016**, *138*, 1010–1016.

(9) Van der Stam, W.; Geuchies, J. J.; Altantzis, T.; Van Den Bos, K. H. W.; Meeldijk, J. D.; Van Aert, S.; Bals, S.; Vanmaekelbergh, D.; De Mello Donega, C. Highly Emissive Divalent-Ion-Doped Colloidal CsPb1-XMxBr3Perovskite Nanocrystals through Cation Exchange. *J. Am. Chem. Soc.* **2017**, *139*, 4087–4097.

(10) Protesescu, L.; Yakunin, S.; Kumar, S.; Bär, J.; Bertolotti, F.; Masciocchi, N.; Guagliardi, A.; Grotevent, M.; Shorubalko, I.; Bodnarchuk, M. I.; et al. Dismantling the “Red Wall” of Colloidal Perovskites: Highly Luminescent Formamidinium and Formamidinium-Cesium Lead Iodide Nanocrystals. *ACS Nano* **2017**, *11*, 3119–3134.

(11) Akkerman, Q. A.; D’Innocenzo, V.; Accornero, S.; Scarpellini, A.; Petrozza, A.; Prato, M.; Manna, L. Tuning the Optical Properties of Cesium Lead Halide Perovskite Nanocrystals by Anion Exchange Reactions. *J. Am. Chem. Soc.* **2015**, *137*, 10276–10281.

(12) Koscher, B. A.; Bronstein, N. D.; Olshansky, J. H.; Bekenstein, Y.; Alivisatos, A. P. Surface- vs Diffusion-Limited Mechanisms of Anion Exchange in CsPbBr3 Nanocrystal Cubes Revealed through Kinetic Studies. *J. Am. Chem.*

Soc. **2016**, *138*, 12065–12068.
(13) Nedelcu, G.; Protesescu, L.; Yakunin, S.; Bodnarchuk, M. I.; Grotevent, M. J.; Kovalenko, M. V. Fast Anion-Exchange in Highly Luminescent Nanocrystals of Cesium Lead Halide Perovskites (CsPbX 3 , X = Cl, Br, I). *Nano Lett.* **2015**, *15*, 5635–5640.
(14) Creutz, S. E.; Crites, E. N.; De Siena, M. C.; Gamelin, D. R. Colloidal Nanocrystals of Lead-Free Double-Perovskite (Elpasolite) Semiconductors: Synthesis and Anion Exchange to Access New Materials. *Nano Lett.* **2018**, *18*, 1118–1123.
(15) Bekenstein, Y.; Dahl, J. C.; Huang, J.; Osowiecki, W. T.; Swabeck, J. K.; Chan, E. M.; Yang, P.; Alivisatos, A. P. The Making and Breaking of Lead-Free Double Perovskite Nanocrystals of Cesium Silver-Bismuth Halide Compositions. *Nano Lett.* **2018**, *18*, 3502–3508.
(16) Berhe, T. A.; Su, W.-N.; Chen, C.-H.; Pan, C.-J.; Cheng, J.-H.; Chen, H.-M.; Tsai, M.-C.; Chen, L.-Y.; Dubale, A. A.; Hwang, B.-J. Organometal Halide Perovskite Solar Cells: Degradation and Stability. *Energy Environ. Sci.* **2016**, *9*, 323–356.
(17) Babayigit, A.; Duy Thanh, D.; Ethirajan, A.; Manca, J.; Muller, M.; Boyen, H.-G.; Conings, B. Assessing the Toxicity of Pb- and Sn-Based Perovskite Solar Cells in Model Organism Danio Rerio. *Sci. Rep.* **2016**, *6*, 18721.
(18) Savory, C. N.; Walsh, A.; Scanlon, D. O. Can Pb-Free Halide Double Perovskites Support High-Efficiency Solar Cells? *ACS Energy Lett.* **2016**, *1*, 949–955.
(19) Slavney, A. H.; Hu, T.; Lindenberg, A. M.; Karunadasa, H. I. A Bismuth-Halide Double Perovskite with Long Carrier Recombination Lifetime for Photovoltaic Applications. *J. Am. Chem. Soc.* **2016**, *138*, 2138–2141.
(20) Volonakis, G.; Filip, M. R.; Haghighirad, A. A.; Sakai, N.; Wenger, B.; Snaith, H. J.; Giustino, F. Lead-Free Halide Double Perovskites via Heterovalent Substitution of Noble Metals. *J. Phys. Chem. Lett.* **2016**, *7*, 1254–1259.
(21) Chakraborty, S.; Xie, W.; Mathews, N.; Sherburne, M.; Ahuja, R.; Asta, M.; Mhaisalkar, S. G. Rational Design: A High-Throughput Computational Screening and Experimental Validation Methodology for Lead-Free and Emergent Hybrid Perovskites. *ACS Energy Lett.* **2017**, *2*, 837–845.
(22) Ganose, A. M.; Savory, C. N.; Scanlon, D. O. Beyond Methylammonium Lead Iodide: Prospects for the Emergent Field of Ns2containing Solar Absorbers. *Chem. Commun.* **2017**, *53*, 20–44.
(23) Jellicoe, T. C.; Richter, J. M.; Glass, H. F. J.; Tabachnyk, M.; Brady, R.; Dutton, S. E.; Rao, A.; Friend, R. H.; Credgington, D.; Greenham, N. C.; et al. Synthesis and Optical Properties of Lead-Free Cesium Tin Halide Perovskite Nanocrystals. *J. Am. Chem. Soc.* **2016**, *138*, 2941–2944.
(24) Liu, F.; Ding, C.; Zhang, Y.; Ripolles, T. S.; Kamisaka, T.; Toyoda, T.; Hayase, S.; Minemoto, T.; Yoshino, K.; Dai, S.; et al. Colloidal Synthesis of Air-Stable Alloyed CsSn 1– x Pb x I 3 Perovskite Nanocrystals for Use in Solar Cells. *J. Am. Chem. Soc.* **2017**, *139*, 16708–16719.
(25) Wong, A. B.; Bekenstein, Y.; Kang, J.; Kley, C. S.; Kim, D.; Gibson, N. A.; Zhang, D.; Yu, Y.; Leone, S. R.; Wang, L. W.; et al. Strongly Quantum Confined Colloidal Cesium Tin Iodide Perovskite Nanoplates: Lessons for Reducing Defect Density and Improving Stability. *Nano Lett.* **2018**, *18*, 2060–2066.
(26) Chen, L. J. Synthesis and Optical Properties of Lead-Free Cesium Germanium Halide Perovskite Quantum Rods. *RSC Adv.* **2018**, *8*, 18396–18399.
(27) Cai, Y.; Xie, W.; Ding, H.; Chen, Y.; Thirumal, K.; Wong, L. H.; Mathews, N.; Mhaisalkar, S. G.; Sherburne, M.; Asta, M. Computational Study of Halide

Perovskite-Derived A 2 BX 6 Inorganic Compounds: Chemical Trends in Electronic Structure and Structural Stability. *Chem. Mater.* **2017**, *29*, 7740–7749.
(28) Wang, A.; Yan, X.; Zhang, M.; Sun, S.; Yang, M.; Shen, W.; Pan, X.; Wang, P.; Deng, Z. Controlled Synthesis of Lead-Free and Stable Perovskite Derivative Cs2SnI6 Nanocrystals via a Facile Hot-Injection Process. *Chem. Mater.* **2016**, *28*, 8132–8140.
(29) Lee, B.; Stoumpos, C. C.; Zhou, N.; Hao, F.; Malliakas, C.; Yeh, C. Y.; Marks, T. J.; Kanatzidis, M. G.; Chang, R. P. H. Air-Stable Molecular Semiconducting Iodosalts for Solar Cell Applications: Cs2SnI6 as a Hole Conductor. *J. Am. Chem. Soc.* **2014**, *136*, 15379–15385.
(30) Saparov, B.; Sun, J. P.; Meng, W.; Xiao, Z.; Duan, H. S.; Gunawan, O.; Shin, D.; Hill, I. G.; Yan, Y.; Mitzi, D. B. Thin-Film Deposition and Characterization of a Sn-Deficient Perovskite Derivative Cs2SnI6. *Chem. Mater.* **2016**, *28*, 2315–2322.
(31) Zhang, Y.; Yin, J.; Parida, M. R.; Ahmed, G. H.; Pan, J.; Bakr, O. M.; Brédas, J.-L.; Mohammed, O. F. Direct-Indirect Nature of the Bandgap in Lead-Free Perovskite Nanocrystals. *J. Phys. Chem. Lett.* **2017**, *8*, 3173–3177.
(32) McCall, K. M.; Stoumpos, C. C.; Kostina, S. S.; Kanatzidis, M. G.; Wessels, B. W. Strong Electron–Phonon Coupling and Self-Trapped Excitons in the Defect Halide Perovskites A 3 M 2 I 9 (A = Cs, Rb; M = Bi, Sb). *Chem. Mater.* **2017**, *29*, 4129–4145.
(33) Pal, J.; Manna, S.; Mondal, A.; Das, S.; Adarsh, K. V.; Nag, A. Colloidal Synthesis and Photophysics of M 3 Sb 2 I 9 (M=Cs and Rb) Nanocrystals: Lead-Free Perovskites. *Angew. Chemie Int. Ed.* **2017**, *56*, 14187–14191.
(34) Yang, B.; Chen, J.; Yang, S.; Hong, F.; Sun, L.; Han, P.; Pullerits, T.; Deng, W.; Han, K. Lead-Free Silver-Bismuth Halide Double Perovskite Nanocrystals. *Angew. Chemie - Int. Ed.* **2018**, *57*, 5359–5363.
(35) Zhou, L.; Xu, Y.-F.; Chen, B.-X.; Kuang, D.-B.; Su, C.-Y. Synthesis and Photocatalytic Application of Stable Lead-Free Cs $_2$ AgBiBr $_6$ Perovskite Nanocrystals. *Small* **2018**, *14*, 1703762.
(36) Connor, B. A.; Leppert, L.; Smith, M. D.; Neaton, J. B.; Karunadasa, H. I. Layered Halide Double Perovskites: Dimensional Reduction of Cs2AgBiBr6. *J. Am. Chem. Soc.* **2018**, *140*, 5235–5240.
(37) Zhou, J.; Xia, Z.; Molokeev, M. S.; Zhang, X.; Peng, D.; Liu, Q. Composition Design, Optical Gap and Stability Investigations of Lead-Free Halide Double Perovskite Cs2AgInCl6. *J. Mater. Chem. A* **2017**, *5*, 15031–15037.
(38) Volonakis, G.; Haghighirad, A. A.; Milot, R. L.; Sio, W. H.; Filip, M. R.; Wenger, B.; Johnston, M. B.; Herz, L. M.; Snaith, H. J.; Giustino, F. Cs2InAgCl6: A New Lead-Free Halide Double Perovskite with Direct Band Gap. *J. Phys. Chem. Lett.* **2017**, *8*, 772–778.
(39) Tran, T. T.; Panella, J. R.; Chamorro, J. R.; Morey, J. R.; McQueen, T. M. Designing Indirect–direct Bandgap Transitions in Double Perovskites. *Mater. Horiz.* **2017**, *4*, 688–693.
(40) Luo, J.; Li, S.; Wu, H.; Zhou, Y.; Li, Y.; Liu, J.; Li, J.; Li, K.; Yi, F.; Niu, G.; et al. Cs2AgInCl6Double Perovskite Single Crystals: Parity Forbidden Transitions and Their Application for Sensitive and Fast UV Photodetectors. *ACS Photonics* **2018**, *5*, 398–405.
(41) Locardi, F.; Cirignano, M.; Baranov, D.; Dang, Z.; Prato, M.; Drago, F.; Ferretti, M.; Pinchetti, V.; Fanciulli, M.; Brovelli, S.; et al. Colloidal Synthesis of Double Perovskite Cs 2 AgInCl 6 and Mn-Doped Cs 2 AgInCl 6 Nanocrystals. *J. Am. Chem. Soc.* **2018**, *140*, 12989–12995.
(42) Goldschmidt, V. M. Die Gesetze Der Krystallochemie. *Naturwissenschaften* **1926**, *14*, 477–485.

(43) Nagabhushana, G. P.; Shivaramaiah, R.; Navrotsky, A. Direct Calorimetric Verification of Thermodynamic Instability of Lead Halide Hybrid Perovskites. *Proc. Natl. Acad. Sci. U. S. A.* **2016**, *113*, 7717–7721.
(44) Sun, Q.; Yin, W. J. Thermodynamic Stability Trend of Cubic Perovskites. *J. Am. Chem. Soc.* **2017**, *139*, 14905–14908.
(45) Travis, W.; Glover, E. N. K.; Bronstein, H.; Scanlon, D. O.; Palgrave, R. G. On the Application of the Tolerance Factor to Inorganic and Hybrid Halide Perovskites: A Revised System. *Chem. Sci.* **2016**, *7*, 4548–4556.
(46) Krieg, F.; Ochsenbein, S. T.; Yakunin, S.; ten Brinck, S.; Aellen, P.; Süess, A.; Clerc, B.; Guggisberg, D.; Nazarenko, O.; Shynkarenko, Y.; et al. Colloidal CsPbX 3 (X = Cl, Br, I) Nanocrystals 2.0: Zwitterionic Capping Ligands for Improved Durability and Stability. *ACS Energy Lett.* **2018**, *3*, 641–646.
(47) Huang, H.; Bodnarchuk, M. I.; Kershaw, S. V; Kovalenko, M. V; Rogach, A. L. Lead Halide Perovskite Nanocrystals in the Research Spotlight: Stability and Defect Tolerance. *ACS Energy Lett.* **2017**, *2*, 2071–2083.
(48) Krieg, F.; Ochsenbein, S. T.; Yakunin, S.; ten Brinck, S.; Aellen, P.; Süess, A.; Clerc, B.; Guggisberg, D.; Nazarenko, O.; Shynkarenko, Y.; et al. Colloidal CsPbX 3 (X = Cl, Br, I) Nanocrystals 2.0: Zwitterionic Capping Ligands for Improved Durability and Stability. *ACS Energy Lett.* **2018**, *3*, 641–646.
(49) Liu, Z.; Bekenstein, Y.; Ye, X.; Nguyen, S. C.; Swabeck, J.; Zhang, D.; Lee, S. T.; Yang, P.; Ma, W.; Alivisatos, A. P. Ligand Mediated Transformation of Cesium Lead Bromide Perovskite Nanocrystals to Lead Depleted Cs4PbBr6 Nanocrystals. *J. Am. Chem. Soc.* **2017**, *139*, 5309–5312.
(50) Tauc, J. Optical Properties and Electronic Structure of Amorphous Ge and Si. *Mater. Res. Bull.* **1968**, *3*, 37–46.
(51) Perdew, J. P.; Burke, K.; Ernzerhof, M. Generalized Gradient Approximation Made Simple. *Phys. Rev. Lett.* **1996**, *77*, 3865–3868.
(52) Kresse, G.; Furthmüller, J. Efficient Iterative Schemes for Ab Initio Total-Energy Calculations Using a Plane-Wave Basis Set. *Phys. Rev. B - Condens. Matter Mater. Phys.* **1996**, *54*, 11169–11186.
(53) Wannier, G. H. The Structure of Electronic Excitation Levels in Insulating Crystals. *Phys. Rev.* **1937**, *52*, 191–197.
(54) Kresse, G.; Furthmüller, J. Efficient Iterative Schemes for Ab Initio Total-Energy Calculations Using a Plane-Wave Basis Set. *Phys. Rev. B - Condens. Matter Mater. Phys.* **1996**, *54*, 11169–11186.
(55) Madsen, G. K. H.; Singh, D. J. BoltzTraP. A Code for Calculating Band-Structure Dependent Quantities. *Comput. Phys. Commun.* **2006**, *175*, 67–71.
(56) Imran, M.; Caligiuri, V.; Wang, M.; Goldoni, L.; Prato, M.; Krahne, R.; De Trizio, L.; Manna, L. Benzoyl Halides as Alternative Precursors for the Colloidal Synthesis of Lead-Based Halide Perovskite Nanocrystals. *J. Am. Chem. Soc.* **2018**, *140*, 2656–2664.
(57) Riedinger, A.; Ott, F. D.; Mule, A.; Mazzoti, S.; Knüsel, P. N.; Kress, S. J. P.; Prins, F.; Erwin, S. C.; Norris, D. J. An Intrinsic Growth Instability in Isotropic Materials Leads to Quasi-Two-Dimensional Nanoplatelets. *Nat. Mater.* **2017**, *16*, 743–748.
(58) Miessler, G. L.; Fischer, P. J.; Tarr, D. A. *Inorganic Chemistry*, Fifth.; Pearson, 2014.
(59) Akkerman, Q. A.; Park, S.; Radicchi, E.; Nunzi, F.; Mosconi, E.; De Angelis, F.; Brescia, R.; Rastogi, P.; Prato, M.; Manna, L. Nearly Monodisperse Insulator Cs4PbX6 (X = Cl, Br, I) Nanocrystals, Their Mixed Halide Compositions, and Their Transformation into CsPbX3 Nanocrystals. *Nano Lett.* **2017**, *17*, 1924–1930.
(60) Palazon, F.; Almeida, G.; Akkerman, Q. A.; De Trizio, L.; Dang, Z.; Prato, M.;

Manna, L. Changing the Dimensionality of Cesium Lead Bromide Nanocrystals by Reversible Postsynthesis Transformations with Amines. *Chem. Mater.* **2017**, *29*, 4167–4171.
(61) Udayabhaskararao, T.; Houben, L.; Cohen, H.; Menahem, M.; Pinkas, I.; Avram, L.; Wolf, T.; Teitelboim, A.; Leskes, M.; Yaffe, O.; et al. A Mechanistic Study of Phase Transformation in Perovskite Nanocrystals Driven by Ligand Passivation. *Chem. Mater.* **2018**, *30*, 84–93.
(62) Parr, R. G.; Pearson, R. G. Absolute Hardness: Companion Parameter to Absolute Electronegativity. *J. Am. Chem. Soc.* **1983**, *105*, 7512–7516.

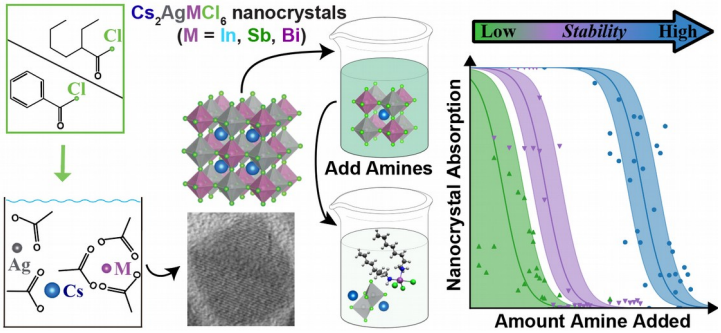

For Table of Contents only